ChemComm

Enhanced Vertical Carrier Mobility in Poly(3-alkylthiophene) Thin Films Sandwiched with Self-assembled Monolayer and Surface-segregated Layer

Journal:	*ChemComm*
Manuscript ID:	CC-COM-12-2013-049760.R2
Article Type:	Communication
Date Submitted by the Author:	12-Feb-2014

Complete List of Authors:	Ma, Jusha; Beijing Institute of Technology, School of Material Science and Engineering; The University of Tokyo, Department of Applied Chemistry, School of Engineering Hashimoto, Kazuhito; The University of Tokyo, Department of Applied Chemistry, School of Engineering Koganezawa, Tomoyuki; Japan Synchrotron Radiation Research Institute, Tajima, Keisuke; RIKEN Center for Emergent Matter Science (CEMS), Supramolecular Chemistry Division; Japan Science and Technology Agency, Precursory Research for Embryonic Science and Technology

Chemical Communications RSCPublishing

COMMUNICATION

Enhanced Vertical Carrier Mobility in Poly(3-alkylthiophene) Thin Films Sandwiched with Self-assembled Monolayer and Surface-segregated Layer

Cite this: DOI: 10.1039/x0xx00000x

Jusha Ma[a,b], Kazuhito Hashimoto[b], Tomoyuki Koganezawa[c], Keisuke Tajima[d,e,*]

Received 00th January 2012,
Accepted 00th January 2012

DOI: 10.1039/x0xx00000x

www.rsc.org/

End-functionalized poly(3-butylthiophene) with a thiol group (P3BT-S) was synthesized and used to form a self-assembled monolayer (SAM). It can induce the end-on orientation in the thin film which has the potential further enhance hole mobility up to 1.1 × 10^{-2} cm^2 V^{-1} s^{-1} in the vertical direction.

The low charge mobility of conjugated polymers compared with inorganic semiconductors has limited their use in polymer-based electronic devices[1]. Recently, charge mobilities in the range of 10^{-1} to 10^{1} cm^2 V^{-1} s^{-1} have been reported for p-type semiconducting polymers in organic field-effect transistors (OFETs)[2]. In OFETs, the charge transport is parallel to the substrate and occurs at the semiconductor/insulator interface[3]. However, in some organic thin-film electronic devices, such as organic light-emitting diodes, organic solar cells, and vertical organic field effect transistors[4], charge carrier conduction perpendicular to the substrate through the bulk film is more important. There are several methods for measuring the hole mobility perpendicular to the substrate [5], but typically the upper limit is 10^{-5} to 10^{-3} cm^2 V^{-1} s^{-1} for conjugated polymers[6]. This difference between the parallel and perpendicular mobilities may arise from the differences in charge density, transport region (bulk vs. interface) and molecular orientations.

Semiconducting polymers have strongly anisotropic structures; therefore, the molecular orientation could substantially affect the transport properties, given that highly ordered crystalline structures can be achieved in films. Planar π-conjugated polymers have three possible orientations: edge-on, where the main chain is parallel and the π-plane is perpendicular to the surface and the substrate; face-on, where the main chain and the π-plane are parallel; and end-on, where the main chain and the π-plane are perpendicular. For perpendicular conduction, the edge-on orientation has a clear disadvantage, because the charge must hop over the insulating side-chains between two adjacent polymers, which would has a large energy barrier. The face-on orientation should allow strong interchain interactions through the π-orbitals and result in better perpendicular transport[7]. The end-on orientation should be the most suitable, because the mobility along the conjugated main chain can theoretically reach more than 600 cm^2 V^{-1} s^{-1}.[8] Although disordered polymer domains between the oriented crystalline domains may act as hopping barriers[9], the average direction of the orientation and the relative orientation of the crystalline domains could substantially affect the perpendicular charge transport in terms of mobility and activation energy[10]. In our previous work[11], we reported the spontaneous surface segregation behaviour of poly(3-butylthiophene) with a semifluoroalkyl chain at one end (P3BT-F) during spin-coating. The polymer adopted an end-on orientation on the top of the thin film and induced the same orientation in the bulk film consisting of non-functionalized poly(3-butylthiophene) (P3BT). However, because of interactions with the substrate and alkyl side chains, domains with an edge-on orientation formed at the bottom of the films. The insulating layer of the side chain and the domain boundaries between the end-on and edge-on regions will hinder further improvement of hole mobility[12]. The perpendicular charge mobility could be increased if the end-on orientation could also be induced at the substrate interface.

In this paper, we report the preparation of a self-assembled monolayer (SAM) based on thiol-terminated poly(3-butylthiophene) (P3BT-S) on a gold surface. Modifying the substrate surface with alkyl-SAMs was expected to induce the edge-on orientation of poly(3-alkylthiophene) (P3AT) films around the interface[13]. The orientation of the P3BT-S SAM

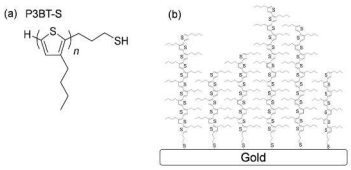

Fig 1. (a) Chemical structure of P3BT-S and (b) schematic of P3BT-S SAMs on a gold surface.

altered the orientation of P3AT at the substrate interface. In addition, P3BT thin films with a surface segregated layer of P3BT-F at the top surface and a P3BT-S SAM on the substrate were prepared. The vertical hole mobility of this sandwich structure was measured by the space-charge limited current (SCLC) and correlated to the proportion of end-on and edge-on orientations in the films evaluated by glazing angle X-ray diffraction (GIXRD).

P3BT-S (Fig. 1a) was synthesized according to the previously reported method for fluoroalkyl-terminated poly(3-butylthiophene) (P3BT-F)[14] and thiol-terminated poly(3-hexylthiophene)[15]. Allyl-terminated P3BT was synthesized by Ni-catalysed polymerization and quenched with an allyl Grignard reagent[16]. The chain end was reacted with thioacetic acid and subsequently hydrolysed. The chemical structure was confirmed by ^{1}H NMR and MALDI-TOF-MS (see ESI). Gel permeation chromatography (GPC) showed the number-average molecular weight (M_n) of P3BT-S was 2100 g mol^{-1} with a polydispersity index of 1.06. The molecular weight with the highest intensity in the MALDI-TOF-MS spectrum was 1734 g mol^{-1}, which corresponds to a degree of polymerization (n) of 12.

The P3BT-S SAM was prepared on a gold surface by immersing the substrate in a toluene solution of P3BT-S using a previously reported method[17]. A schematic of the P3BT-S SAM structure is shown in Fig 1b. The adsorption of P3BT-S on a gold surface was examined by X-ray photoelectron spectroscopy (XPS). The C 1s and S 2s peaks from P3BT-S on the gold surface were observed after the substrate was treated. Furthermore, the XPS depth profile showed the thickness of the P3BT-S layer was less than 5 nm. Atomic force microscopy showed that the surface was relatively flat and no large aggregates were observed. The root mean square of the surface roughness changed from 0.6 to 1.2 nm after the adsorption of P3BT-S on the gold surface.

The P3BT-S layer was also analysed quantitatively by spectral ellipsometry (SE) and X-ray reflectivity (XRR). The SE results show that the fittings with tan Ψ and cos Δ were good for a 4.86-nm-thick P3BT-S layer. The refractive index n and extinction coefficient k used in this fitting was presented in ESI. The XRR measurement showed clear interference fringes and the fitting of the data indicated that the thickness of P3BT-S on gold was 4.45 nm with a density of 0.98 g cm^{-3} (see ESI). The density of close packed P3BT calculated from the diffraction experiments has been reported as 1.22-1.29 g cm^{-3}.[18] Based on this, the surface coverage of P3BT-S was estimated as 76-80% of the closed packed structure. Both SE and XRR showed similar thicknesses for the P3BT-S layer. The full extended conformation of P3BT-S with a degree of polymerization of n = 12 was calculated from the molecular model as 4.8 nm, which is comparable to the SE and XRR results. This suggests that the adsorbed molecules were oriented almost perpendicularly to the substrate.

The amount of P3BT-S adsorbed on the gold substrate was measured by a quartz crystal microbalance (QCM) during adsorption as 460 ng cm^{-2} at equilibrium. Compared to the calculated value based on the assumption that P3BT-S fully covers the gold substrate with a close packed structure and end-on orientation (582 ng cm^{-2}), the surface coverage was 79%. This is consistent with the surface density observed by XRR. When P3BT was used in solution, the amount adsorbed was much smaller (78 ng cm^{-2}), suggesting that thiol group at the chain end, not the thiophene sulfur, functions as the anchor to the gold surface as in ordinary alkanethiol SAMs. Based on these results, we conclude that P3BT-S forms SAMs on a gold substrate with a relatively high density and an orientation nearly perpendicular to the substrate.

To determine the effect of P3BT-S SAMs on the orientation of the polymer chains in the films at the SAM/polymer interface, P3BT was spin-coated on the gold substrate coated with a P3BT-S SAM. The chain orientation of the film was investigated by in-plane and out-of-plane GIXRD measurements. The P3BT-S SAMs did not show any diffraction signals, which suggests the lateral packing order of the P3BT-S SAMs was weak. This may be because of the low coverage of P3BT-S on gold, the roughness of the gold surface, the backbone of P3BT-S being too short, or a broad orientation distribution. Here we focus on the effect of P3BT-S SAMs on inducing an end-on orientation in the films. The in-plane and out-of-plane GIXRD patterns of the P3BT films spin-coated on a P3BT-S SAM and on the bare gold substrate are shown in Fig. 2a and b, respectively. The P3BT film on the gold substrate only shows a π-π stacking peak at 23.2° (3.8 Å) in the in-plane pattern and strong lamellar peaks in the out-of-plane pattern at 6.6° (13.4 Å), indicating that the orientation is mostly edge-on. The P3BT film on the P3BT-S SAM shows both a π-π stacking peak and a lamellar peak in the in-plane pattern, suggesting the end-on orientation. The absence of the π-π stacking peak in the

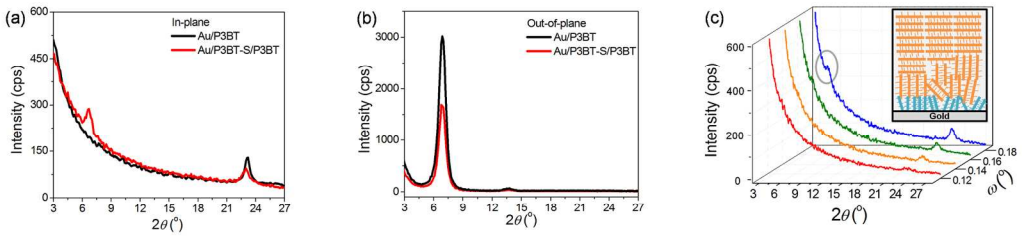

Fig 2. (a) In-plane, and (b) out-of-plane GIXRD patterns of P3BT and P3BT-S/P3BT films. (c) In-plane GIXRD patterns of the P3BT-S/P3HT film with ω of 0.12-0.18°. Circles indicate the appearance of the P3HT lamellar peak. Inset: schematic of the P3BT-S/P3HT film. Blue rods represent P3BT- S and orange represent P3HT.

out-of-plane pattern also suggests that the orientation is the end-on, not the face-on. The lamellar peak was still observed in the out-of-plane pattern, although the intensity was about half that of the P3BT film on gold, suggesting that the P3BT-S SAM reduced the fraction of the edge-on orientation in the P3BT film.

Next, the location of the two perpendicular orientations was investigated by changing the incident angle, ω, of the GIXRD measurements, because the depth of the X-ray penetration into the films depends on ω[19]. The P3HT film spin-coated on P3BT-S SAMs was used instead of P3BT, because for the lamellar peaks P3HT gives *d*-spacings different from those of P3BT and avoids the possible contribution from the diffraction of the bottom P3BT-S layer. Fig. 2c shows the in-plane GIXRD measured by gradually varying ω from 0.12 to 0.18° (critical angle of P3HT: α_c = 0.158° for λ = 1.54 Å). When ω was greater than 0.16°, the P3HT lamellar peak at 5.2° (17.0 Å) began to appear, indicating that the P3HT end-on orientation was present close to only the substrate and not the surface. This behaviour is the opposite of the P3BT-F surface segregated layer we have observed previously[11]. This suggests that the end-on orientation of P3HT was induced from the P3BT-S SAMs at the bottom of the film. Inset of Fig. 2c shows a schematic of the P3BT-S/P3HT film. The lower surface energy of the alkyl side chains could induce the edge-on orientation at the surface during the spin-coating. However, P3BT-S SAMs at the bottom probably affected the orientation of P3AT by cocrystallization to produce the perpendicular orientation from the interface and reduce the fraction of the edge-on orientation.

We combined the surface segregated layer and the P3BT-S SAM to induce the end-on orientation in the bulk film more efficiently. The chain orientation and orientation distribution were measured by GIXRD using a synchrotron radiation source and a 2-D image detector. The 2-D GIXRD images of P3BT, P3BT-S/P3BT, and P3BT-S/P3BT/P3BT-F films are compared in Fig. 3a. The appearance of the end-on orientation in P3BT-S/P3BT and P3BT-S/P3BT/P3BT-F films is clearly visible (q_{xy} = 4.8 nm^{-1} and *d*-spacing = 13.1 Å for the lamellar (100) peak). The weakening of the edge-on orientation in these two films is also visible (q_z = 10.0 nm^{-1} and *d*-spacing = 6.3 Å for the lamellar (200) peak). Quantitative analysis of this orientation change was performed by integrating the lamellar peak intensity along the q_{xy} and q_z axes.

We observed a clear trend in the change in the lamellar peak intensity that reflected the amount of an orientation in the thin films. Fig. 3b shows the fraction of the end-on orientation in thin films increased from P3BT to P3BT-S/P3BT and to P3BT-S/P3BT/P3BT-F. At the same time, the fraction of the edge-on orientation decreased. A similar change was observed for P3BT-S/P3HT/P3BT-F films (see ESI). Secondly, the inclination orientation distribution of the edge-on lamellar (100) peak in the P3BT-S/P3BT/P3BT-F film was significantly larger compared with the P3BT-S/P3BT and P3BT films (q_z = 5.0 nm^{-1} and d-spacing = 12.6 Å). Fig. 3c shows the dependence of the peak intensity on the azimuth angle □. The P3BT-S/P3BT/P3BT-F film shows a broader diffraction peak from the lamellar structure compared to P3BT or P3BT-S/P3BT films, suggesting that the P3BT-S/P3BT/P3BT-F film has a large directional disorder in the edge-on orientation.

These results indicate that using both the surface segregated P3BT-F layer at the top and the P3BT-S SAM at the bottom of the film increases the fraction of the end-on orientation and decreases that of the edge-on orientation in the P3BT film bulk. It also increases the orientation distribution of the edge-on orientation.

The electrical conductivity of the films perpendicular to the substrate was investigated by SCLC measurements. Hole-only devices were fabricated with a structure of Au/polymer film/MoO_3/Au. The hole mobility was calculated from SCL region in the *J-V* curve by the Mott–Gurney square law[20]. Activation energy for the conduction was estimated by measuring the temperature dependence of the *J-V* characteristics using the thermally activated transport model (see ESI for the details of the measurements). The results are summarized in Table 1. The P3BT film had an average mobility of 9.6 × 10^{-4} cm^2 V^{-1} s^{-1}, which is typically observed in P3AT spin-coated films by the SCLC method[21]. Using the P3BT-S SAM on the bottom electrode increased the mobility to 1.8 × 10^{-3} cm^2 V^{-1} s^{-1}. Using only the surface segregated P3BT-F layer a mobility of 4.0 × 10^{-3} cm^2 V^{-1} s^{-1} can be achieved. It has been reported that lower molecular weight P3BT achieved a mobility of 1.6 × 10^{-3} cm^2 V^{-1} s^{-1}. Interestingly, using both the P3BT-S SAM and the P3BT-F surface layer led to a much higher hole mobility of 1.1 × 10^{-2} cm^2 V^{-1} s^{-1}. To our knowledge, this is the highest mobility reported for P3AT-

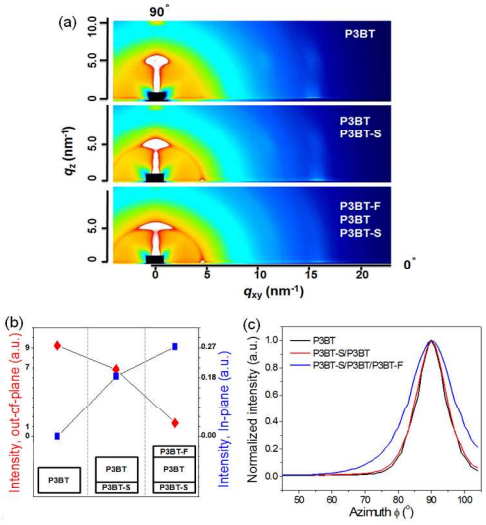

Fig 3. (a) 2D GIXRD images of P3BT, P3BT-S/P3BT, and P3BT-S/P3BT/P3BT-F thin films (from top to bottom). (b) Out-of plane diffraction intensity calculated from the double integral of the edge-on lamellar (100) peak (R_q = 4.8-5.2 nm^{-1} and ϕ = 85-90°) (red diamonds) and the in-plane diffraction intensity calculated from the double integral of the end-on lamellar (100) peak R_q = 4.6-5.0 nm^{-1} and ϕ = 1-6° (blue squares), where R_q is the radius from the diffraction center, ϕ is the azimuth angle from the q_{xy} plane (ϕ = 0°) to the q_z plane (ϕ = 90°). (c) Diffraction intensity at a q_z of 5.0 nm^{-1} as a function of the azimuth angle, ϕ, for the P3BT, P3BT-S/P3BT, and P3BT-S/P3BT/P3BT-F films. The intensities were normalized at ϕ = 90° for comparison.

based semiconducting polymers perpendicular to the substrate [22].

The activation energy of hole conduction in the P3BT-S/P3BT/P3BT-F film was 80 meV, which is significantly lower than that in the P3BT, P3BT-S/P3BT, and P3BT/P3BT-F films (130-160 meV). This result indicates that the same factors limit the transport for films that contain large continuous edge-on orientation domains either at the top or at the bottom of the film. This could be explained by an increase in the favourable percolation path along the polymer backbone in the P3BT-S/P3BT/P3BT-F film forming a more continuous and efficient path for charge transport, resulting in a different activation energy[10]. A further factor might be a difference in the energy barrier caused by the different relative orientation of adjacent grains, because the grain boundaries along the polymer backbone could provide easier charge transport compared with other boundaries[12]. For example, the boundaries between two end-on grains may have a lower energy barrier for hopping compared to that between edge-on and end-on grains or two edge-on grains.

When P3HT was used instead of P3BT, the mobility was increased from 2.9×10^{-4} to 7.6×10^{-3} cm^2 V^{-1} s^{-1} by using both the top and bottom layers, which is about a 25-fold increase (Table 1). The difference of hole mobility between P3HT and P3BT was smaller when both the top and the bottom layers were used, which could imply more charge transport through the main chains in the sandwiched films instead of the charge hopping through the side chains due to end-on orientation.

We demonstrated that P3BT-S formed an SAM on a gold surface, and that it can change the backbone orientation of spin-coated polymers from an edge-on to an end-on orientation. Our method could be applied to many semicrystalline semiconducting polymers for various organic electronics devices that require vertical charge transportation.

Table 1. hole mobility (μ_h) at room temperature (298 K) and activation energy of the transport (Δ) calculated from variable temperature measurements.

Sample	μ_h (cm^2 V^{-1} s^{-1})	Δ (meV)
P3BT[a]	$(9.6 \pm 0.9) \times 10^{-4}$	151 ± 4
P3BT-S/P3BT[a]	$(1.8 \pm 0.3) \times 10^{-3}$	149 ± 2
P3BT[a]/P3BT-F	$(3.6 \pm 0.5) \times 10^{-3}$	133 ± 2
P3BT-S/P3BT[a]/P3BT-F	$(1.1 \pm 0.2) \times 10^{-2}$	80 ± 3
P3HT[b]	$(2.9 \pm 0.4) \times 10^{-4}$	-
P3BT-S/P3HT[b]/P3BT-F	$(7.6 \pm 1.1) \times 10^{-3}$	-

[a]M_n = 17.8 kg mol^{-1} and PDI = 1.15 by GPC. [b]M_n = 16.3 kg mol^{-1} and PDI = 1.08 by GPC.

Notes and references

[a] *School of Material Science and Engineering, Beijing Institute of Technology, 5 South Zhongguancun Street, Beijing 100081, China*
[b] *Department of Applied Chemistry, School of Engineering, The University of Tokyo, 7-3-1 Hongo, Bunkyo-ku, Tokyo 113-8656, Japan*
[c] *Japan Synchrotron Radiation Research Institute, 1-1-1, Kouto, Sayo-cho, Sayo-gun, Hyogo 679-5198, Japan*
[d] *Japan Science and Technology Agency, Precursory Research for Embryonic Science and Technology, 4-1-8 Honcho, Kawaguchi, Saitama 332-0012, Japan*
[e*] *RIKEN Center for Emergent Matter Science (CEMS), 2-1 Hirosawa, Wako, Saitama 351-0198, Japan, keisuke.tajima@riken.jp*

† Electronic Supplementary Information (ESI) available: Characterization of P3BT-S and P3BT-S SAMs, Experimental details of film bulk orientation by GIXRD and hole mobility and activation energy by SCLC. See DOI: 10.1039/b000000x/

1. S. R. Forrest, *Nature*, 2004, **428**, 911-918.
2. B.-G. Kim, E. J. Jeong, J. Chung, S. Seo, B. Koo and J. Kim, *Nature Mater.*, 2013, **12**, 659-664.
3. Q. Wei, K. Hashimoto and K. Tajima, *ACS Appl. Mater. Interfaces*, 2011, **3**, 139-142.
4. S. Fujimoto, K. Nakayama and M. Yokoyama, *Appl. Phys. Lett.*, 2005, **87**, 133503.
5. A. Kokil, K. Yang and J. Kumar, *J. Polym. Sci. Part B Polym. Phys.*, 2012, **50**, 1130-1144.
6. A. Saeki, Y. Koizumi, T. Aida and S. Seki, *Acc. Chem. Res.*, 2012, **45**, 1193-1202.
7. X. Guo, N. Zhou, S. J. Lou, J. Smith, D. B. Tice, J. Hennek, R. o. P. Ortiz, J. T. L. p. Navarrete, S. Li, J. Strzalka, L. X. Chen, R. P. H. Chang, A. Facchetti and T. J. Marks, *Nature Photonics,* 2013, **7**, 825-833.
8. F. C. Grozema and L. D. A. Siebbeles, *J. Phys. Chem. Lett*., 2011, **2**, 2951-2958.
9. V. Coropceanu, J. r. m. Cornil, D. A. d. S. Filho, Y. Olivier, R. Silbey and J.-L. Bre´das, *chem. Rev.*, 2007, 926-952.
10. B. O'Connor, R. J. Kline, B. R. Conrad, L. J. Richter, D. Gundlach, M. F. Toney and D. M. DeLongchamp, A*dv. Funct. Mater.,* 2011, **21**, 3697-3705
11. J. Ma, K. Hashimoto, T. Koganezawa and K. Tajima, *J. Am. Chem. Soc.*, 2013, **135**, 9644-9647.
12. L. H. Jimison, M. F. Toney, I. McCulloch, M. Heeney and A. Salleo, *Adv. Mater.*, 2009, **21**, 1568-1572.
13. R. Joseph Kline, M. D. McGehee and M. F. Toney, *Nature Mater.*, 2006, **5**, 222-228.
14. J. Ma, Y. Geng, K. Hashimoto and K. Tajima, *Macromol. Chem. Phys.*, 2013, **214**, 1326-1331.
15. E. B. Pentzer, F. A. Bokel, R. C. Hayward and T. Emrick, *Adv. Mater.*, 2012, **24**, 2254 - 2258.
16. M. Jeffries-El, G. v. Sauve´ and R. D. McCullough, *Macromolecules*, 2005, **38**, 10346-10352.
17. J. C. Love, L. A. Estroff, J. K. Kriebel, R. G. Nuzzo and G. M. Whitesides, *Chem. Rev.*, 2005, **105**, 1103-1169.
18. P. Arosio, M. Moreno, A. Famulari, G. Raos, M. Catellani and S. V. Meille, *Chem. Mater.*, 2009, **21**, 78-87.
19. M. Birkholz, *Thin Film Analysis by X-Ray Scattering*, WILEY-VCH, Weinheim, 2006, pp.161-165.
20. Stallinga, *Electrical Characterization of Organic Electronic Materials and Devices,*Wiley, Cornwall, 2009, pp.45-64.
21. G. Lu, H. Tang, Y. Huan, S. Li, L. Li, Y. Wang and X. Yang, A*dv. Funct. Mater.,* 2010, **20**, 1714-1720.
22. J. Ge, M. He, X. Yang, Z. Ye, X. Liu and F. Qiu, *J. Mater. Chem.,* 2012, **22**, 19213.